THE JOURNAL OF PHYSICAL CHEMISTRY A
A JOURNAL OF THE AMERICAN CHEMICAL SOCIETY

pubs.acs.org/JPCA

Article

Metric-Based Assessment Method for MS-T Formalism with Small Subsets of Torsional Conformers

Yicheng Chi, Qinghui Meng, Chengming He, and Peng Zhang*

Cite This: J. Phys. Chem. A 2022, 126, 8305−8314

Read Online

ACCESS | Metrics & More | Article Recommendations | Supporting Information

ABSTRACT: The multi-structural approximation with torsional anharmonicity (MS-T) method and its variants have been widely used for calculating conformational−rovibrational partition functions of large molecules. The present work aimed to propose a systematic method to assess and explain the performance of various variants of the MS-T method. First, we proposed the simplest variant MS-T(2NN) (two nearest neighborhood torsions are coupled) and systematically validated it for large alkanes n-C_nH_{2n+2} (n = 6−10) and their transition states of hydrogen abstraction reactions. Second, we proposed a metric-based method to explain the underlying reason for the good performance of MS-T(2NN)—it includes the torsional conformers that have dominant contributions to the partition function calculations. These conformers are closer to the lowest-energy conformer in the space of dihedral and energy metrics. Third, the same observation and explanation apply to the other two variants, MS-2DT (any two torsions are coupled) and MS-3DT (any three torsional are coupled), which contain increasingly more torsional conformers than MS-T(2NN) but are subsets of the complete set of torsional conformers considered by the MS-T method. Overall, the present method provides a mathematically rigorous and computationally effective diagnosis tool to assess various MS-T methods dealing with the torsional anharmonicity of large molecules in the partition function calculation.

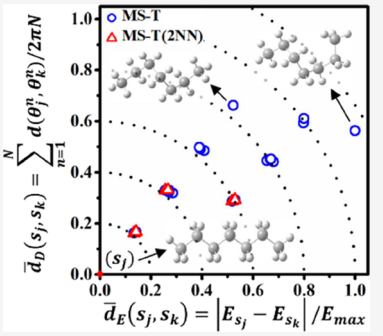

1. INTRODUCTION

The contemporary concerns on energy security and environment protection spawned continuous studies on developing advanced combustion engines to satisfy the increasingly higher requirements for high efficiency and low emissions.[1] There is accordingly a need to carry out comprehensive and systematic research on the combustion chemistry of petroleum-based fuels. However, it is quite challenging to study the thermochemistry and chemical kinetics of these fuels[2−4] on account of their complex components, because they generally consist of hundreds of different hydrocarbon molecules, and large n-alkanes are one of the primary components.[1−7]

There are two crucial factors in the calculation of thermochemistry and chemical kinetics of large n-alkanes, namely, the single-point energy and the partition function. For example, the hydrogen abstraction reaction from an n-alkane by a hydrogen atom, RH + H → R˙ + H_2, has a distinct energy barrier along its reaction coordinate, and the transition state theory (TST) predicts its high-pressure limit rate coefficient as:[8−10]

$$k(T) = \frac{k_B T}{h}\frac{Q^{\dagger}}{Q_{RH}Q_H}\exp\left(-\frac{E^{\dagger}}{k_B T}\right) \quad (1)$$

where Q is the partition function, E is the energy barrier, the superscript "†" denotes the transition state, and k_B, T, and h are the Boltzmann constant, temperature, and the Planck constant, respectively. The uncertainty of the theoretical reaction rate constant is significantly affected by the accuracy of the energy barrier (particularly at relatively low temperatures) and partition functions (particularly at relatively high temperatures).

In recent years, there are extensive theoretical studies on high-level single-point energy calculation of large molecules. Based on the well-known ONIOM (our own N-layered integrated molecular orbital and molecular mechanics),[11] Zhang et al.[12,13] proposed a two-layer ONIOM method, in which the QCISD(T)/CBS and DFT/6-311++G(d,p) methods are used for the high layer and the low layer, respectively. Li et al.[14] developed a generalized energy-based fragmentation (GEBF) approach, in which a large molecule is divided into small fragments and the total energy of the large molecule is obtained from synthesizing the small fragments. Wu et al.[15] proposed a cascaded group-additivity (CGA) ONIOM method by combining the group additivity and two-layer ONIOM methods, in which a large molecule is partitioned into cascaded individual groups and the ONIOM method is used for their energy calculations.

Received: July 5, 2022
Revised: October 12, 2022
Published: October 27, 2022

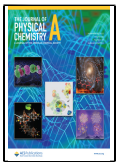

https://doi.org/10.1021/acs.jpca.2c04724
J. Phys. Chem. A 2022, 126, 8305−8314

For calculating partition functions, a common approach is to assume the separability of various modes (degrees of freedom) of external and internal motions, which leads to the additivity of their energies and, in turn, the multiplicativity of their partition functions as such

$$Q = Q_{trans}Q_{rot}Q_{vib}Q_{elec} \quad (2)$$

where the translational (Q_{trans}), rotational (Q_{rot}), vibrational (Q_{vib}), and electronic (Q_{elec}) partition functions can be separately calculated. Generally, vibrational modes can be treated by using the harmonic oscillator (HO) approximation. However, using the HO approximation to treat those torsional modes with relatively low frequencies will result in large errors, particularly at relatively high temperatures.

Extensive studies have been conducted to deal with low-frequency torsional modes. Pitzer and Gwinn[16] performed a seminal work on the one-dimensional hindered rotor (1D-HR) treatments and their subsequent works[17,18] also had far-reaching effects on later studies.[19−22] The Pitzer−Gwinn-like methods have been widely adopted in dealing with torsional anharmonicity in partition function calculations.[23−27] The applicability of the 1D-HR approach relies on the two approximations: the torsions are decoupled and each torsion corresponds to (therefore is used to replace) a specific normal mode. However, torsions are often coupled with each other in a large molecule, and it is difficult (even impossible) to establish one-to-one correspondence between the low-frequency torsions and normal modes. As a result, there is a natural idea to treat torsional coupling by constructing the high-dimensional torsional potential energy surface (PES), which makes a more accurate treatment possible at the cost of the high computational load.[28,29]

Zheng et al.[30] proposed a new class of methods called multi-structural (MS) methods. The methods need neither to calculate high-dimensional torsional PES nor to manually correspond each torsion to a normal mode.[31−34] Instead, the MS methods use the Voronoi tessellation to divide the high-dimensional torsional PES into a number of Voronoi cells around local minima on the torsional PES; in each of the cells, the high-dimensional integral of the classical partition function can be analytically expressed by virtue of the geometric and frequency information of stationary points (local minima and saddle points) on the torsional PES. An open-source code MSTor was developed based on the multi-structural approximation with torsional anharmonicity (referred to as MS-T hereinafter) and has been extensively used in many gas-phase chemical reaction systems.[30,31,34−36]

One of the key procedures in the MS-T calculations is to identify all torsional conformers on the high-dimensional torsional PES. A common approach for this is to generate initial-guess structures for all torsions and then to rule out the identical structures from the results of geometry optimization. Each torsion (excluding the methyl groups) is rotated by 0, 120, and −120° to generate initial-guess structures, and therefore, 3^N initial-guess structures are needed for a hydrocarbon molecule with N non-methyl torsions.[32] Apparently, a huge number of geometry optimization calculations are needed by applying the MS-T method to large molecules. For example, common diesel fuel ranges approximately from $C_{10}H_{20}$ to $C_{15}H_{28}$.[37] Taking n-decane as an example, the MS-T method needs to generate $3^7 = 2187$ initial-guess structures for geometry optimization calculations, and the conformational search of n-decane is computationally affordable at a relatively lower level of theory. However, the research results are not always consistent among different levels, and the subsequent refinement calculations at a higher level of theory are often computationally demanding. Therefore, identifying distinguishable structures among these optimized structures is another challenging work and usually manually formidable, especially for the larger molecules with more torsions, for example, 19,683 initial-guess structures for n-dodecane.

To reduce the computational load of the MS-T method, Bao et al.[38] proposed a cost-effective method to approximate the MS-T partition function, called the dual-level electronic structure method, in which a low-level method is used to optimize all initial-guess structures first, and then a high-level method is used to re-optimize some of the distinguishable structures in order of increasing energy identified by a low-level method. They studied a transition state structure of the hydrogen abstraction of ketohydroperoxide by OH radical, in which the 7 non-methyl torsions generate 2187 initial-guess structures. Although the dual-level method can reduce the computational cost to a certain extent, it still has to deal with a huge number of optimized structures, particularly in large molecular systems. Wu et al.[39] proposed a multi-structural 2-dimensional torsion (MS-2DT) method, which considers all pairs of torsions to generate initial-guess structures, reducing the number of initial-guess structures from 3^N to $9N(N-1)/2$. They used the MS-2DT method to study 18 alkanes (C_6−C_8), and the results are in good agreement with the original MS-T method.

Regardless of the noticeable success of the MS method and its variants in calculating partition functions accurately and efficiently, some critical questions remain to be answered: Do we really need a complete set of distinguishable torsional conformers for the partition function calculation? Can we find an appropriately chosen small subset of distinguishable torsional conformers, which can significantly reduce the computational cost while retaining acceptable accuracy? How do we assess the performance of various subsets (the complete set can be treated as a subset of itself)? In the present work, we proposed the simplest variant MS-T(2NN) and a metric-based method to answer the above questions, particularly the last question that determines our answers to the first two. We shall expatiate the simplest variant MS-T(2NN) and metric-based methods in Section 2, followed by the validation in Section 3, in which we compared the MS-T and MS-T(2NN) methods in the systems of n-C_nH_{2n+2} + H (n = 6−7). In addition, we used the MS-T(2NN) method to study larger n-alkanes (n = 8−10) and compared the entropy results with the literature data. The other variants of the MS-T method, the MS-2DT and MS-3DT methods, are also considered to verify the findings by the metric-based method.

2. THEORETICAL METHODS

2.1. Multi-Structural (MS) Method. In the MS method,[30] the quantum-mechanical torsional partition function is approximated by a classical mechanical configuration integral[18] as

https://doi.org/10.1021/acs.jpca.2c04724
J. Phys. Chem. A 2022, 126, 8305−8314

$$Q^{CM} = \left(\frac{1}{2\pi\beta\hbar^2}\right)^{t/2} (\det\{\boldsymbol{D}\})^{1/2} \int_0^{2\pi/\sigma_1} \dots \int_0^{2\pi/\sigma_t} d\phi_1 \dots d\phi_t e^{-\beta V(\phi_1,\dots,\phi_t)} \quad (3)$$

where $\beta = 1/k_B T$, k_B is the Boltzmann constant, T is the temperature, $\hbar$ is the reduced Planck constant, $\boldsymbol{D}$ is the torsional kinetic energy matrix that evaluated at the global minimum, ϕ_τ is the torsional internal coordinate, σ_τ is the parameter characterizing the periodicity of torsional space, and t is the total number of coupled torsions.

Because of the existence of many local minima that contribute to the evaluation of the partition function, the entire torsional space can be divided into a certain number of distinct subspaces, which correspond to each local minimum, and such that the total partition function is a summation of all the local minima. For a certain torsion τ corresponding to each structure j, the PES is assumed to be described by a periodic function, $V_{j,\tau} = U_j + W_{j,\tau}\{1 - \cos[M_{j,\tau}(\phi_\tau - \phi_{\tau,\mathrm{eq},j})]\}/2, M_{j,\tau}(\phi_\tau - \phi_{\tau,\mathrm{eq},j}) \in [-\pi, \pi]$, where U_j and $\phi_{\tau,\mathrm{eq},j}$ are the potential energy and the torsional internal coordinate, respectively, of the jth local minimum, and $M_{j,\tau}$ is the periodicity parameter. $W_{j,\tau}$ is the effective barrier height estimated by $W_{j,\tau} = 2I_{j,\tau}\omega_{j,\tau}^2/M_{j,\tau}^2$, where $\omega_{j,\tau}$ is the frequency and $I_{j,\tau}$ is the internal moment of inertia. The PES within a certain structure j is assumed to be separable so that $V_j(\phi_1, \dots, \phi_t) \approx \sum_{\tau=1}^{t} V_{j,\tau}(\phi_\tau)$.

The assignment of $M_{j,\tau}$ is an essential part of the MS method. For nearly separable torsions with approximately evenly distributed local minima, $M_{j,\tau}$ simply equals to the total number of local minima in the specific torsion. For strongly coupled (SC) torsions, $M_{j,\tau}$ is determined by the Voronoi tessellation, in which $M_{j,\tau}$ is replaced by M_j^{SC} and assumed to be equivalent in every SC torsion. Then, the local periodicity $M_{j,\tau}$ is defined by $M_{j,\tau} = M_j^{SC} = 2\pi(\Omega_j^{SC})^{-1/t_{SC}}$, where Ω_j^{SC} is the hypervolume of the jth subspace and t_{SC} is the total number of SC torsions. Overall, there are three main roles of $M_{j,\tau}$ in the method. First, it controls the local periodicity. Second, it determines the integral subspace for a specific structure. Third, it accounts for the evaluation of implicit barrier heights.

The conformational−rovibrational partition function obtained by the MS method based on uncoupled torsional potential, MS-T(U),[30] is $Q_{con-rovib}^{MS-T(U)} = \sum_{j=1}^{J} Q_{rot,j}\exp(-\beta U_j) Q_j^{HO} Z_j \prod_{\tau=1}^{t} f_{j,\tau}$, where $Q_{rot,j}$ is the classical rotational partition function of structure j, Q_j^{HO} is the usual normal-mode HO vibrational partition function calculated at structure j, Z_j is a factor designed to ensure that the MS-T(U) partition function reaches the correct high-temperature limit, and $f_{j,\tau}$ is a torsional anharmonicity factor, and based on coupled torsional potential, MS-T(C),[31] is $Q_{con-rovib}^{MS-T(C)} = \sum_{j=1}^{J} Q_{rot,j}\exp(-\beta U_j) Q_j^{HO} \prod_{\tau=1}^{t} f_{j,\tau}$, unlike the MS-T(U) method, $f_{j,\tau}$ is a correction factor that takes account of torsional anharmonicity of the coupled torsions.

2.2. Metric-Based Method. As discussed in the preceding section, identifying all possible distinguishable local minima is crucial in the MS method because it affects the Voronoi tessellation, the local PES, and in turn the partition function. Previous studies have shown that the calculation of the partition function by using the MS method is sensitive to the number of identified local minima.[38,39]

The central idea of the metric-based method to be expatiated below is to mathematically quantify the "similarity" or "closeness" of two torsional conformers and then to quantify the contribution of a conformer to the calculation of the partition function. In previous studies, two optimized structures were considered distinguishable if they have at least one different dihedral angle of torsion or if they have different single-point energies. Additional treatments should be given to the optical isomers. It is apparently unfeasible to manually distinguish all optimized structures because the total number of comparisons for each pair of structures is $N + 1$, including N comparisons of dihedral angles and one comparison of energy, and that for all structures is $(N + 1)M(M - 1)/2$, where M is the total number of optimized structures. Although computer programs can be developed to identify distinguishable conformers, the computational load is significant for usually very large M. For example, the total number of comparisons is about $3^{15} \approx 1.4 \times 10^7$ for $N = 7$ (e.g., n-decane).

Inspired by the mathematical concept of metric or distance function,[40,41] we defined a dihedral metric and an energy metric to quantify the difference between any two structures. For two structures s_j and s_k, where $j \neq k$, the dihedral metric $d_D(s_j, s_k)$ is defined by

$$d_D(s_j, s_k) = \sum_{n=1}^{N} d(\theta_j^n, \theta_k^n) \quad (4)$$

where θ_j^n is the dihedral angle corresponding to the nth torsion of the structure s_j and $d(\theta_j^n, \theta_k^n)$ is a function accounting for the difference of two corresponding dihedral angles:

$$d(\theta_j^n, \theta_k^n) = \min\{|\theta_j^n - \theta_k^n|, |\theta_j^n - \theta_k^n + 2\pi|, |\theta_j^n - \theta_k^n - 2\pi|\} \quad (5)$$

Equation 4 can be treated as a high-dimensional variant of the "Manhattan distance".[42−44] As a metric, $d_D(x, y)$ must satisfy the three axioms such as (1) $d_D(x, y) \geq 0$ and the equality holds only for $x = y$; (2) $d_D(x, y) = d_D(y, x)$; and (3) $d_D(x, y) \leq d_D(x, z) + d_D(z, y)$.[45,46] No cases were found to violate the above three metric axioms in our computational results.

Considering two structures of the same energy may have different dihedral metrics, such as the optical isomers. We defined the energy metric by

$$d_E(s_j, s_k) = |E_{s_j} - E_{s_k}| \quad (6)$$

where E denotes the single-point energy. It is readily seen that the energy metric satisfies all three metric axioms. In the present metric-based method, two structures are considered similar or close if their dihedral and energy metrics are small. The "smallness" of a metric can be so determined that the calculation results reach a prescribed accuracy.

It is noted that the low-energy structures contribute to the partition function significantly more than the high-energy structures, because the Boltzmann factor $e^{-\Delta E/kT}$ is significantly small, for a large $\Delta E = E - E_{min}$, where E_{min} is the single-point energy of the lowest-energy conformer. For example, the contribution of a higher-energy conformer to the total partition function is about 13.5% (at $T = 1000$ K) and 1.8% (at $T = 500$

https://doi.org/10.1021/acs.jpca.2c04724
J. Phys. Chem. A 2022, 126, 8305−8314

K) of that of the lower-energy conformer if ΔE is 2 kcal/mol. However, it should be mentioned that the high-energy structures that have more "loose" modes may also make a larger contribution to the partition function than the low-energy structures at high temperatures.[47,48] Aside from the relative energy of the structure, we thought about the dihedrals of the structure that contain information about the "looseness" or "tightness" of the structure, which can reflect the entropy effects. Meanwhile, these high-energy structures usually only result in errors about a factor of two in the partition function calculation by using the MS-T method.[38,39] Consequently, a complete set of distinguishable local minima could be unnecessary for the purpose of the partition function calculation since many local minima might have a negligible contribution to the partition function. Thus, an ideal way to reduce the computational cost while retaining the computational accuracy is to find those local minima close to the lowest-energy one.

For the convenience of the analysis to be discussed in the following sections, the dihedral and energy metrics can be normalized by

$$\bar{d}_{\mathrm{D}}(s_j, s_k) = d_{\mathrm{D}}(s_j, s_k)/2\pi N \tag{7}$$

$$\bar{d}_{\mathrm{E}}(s_j, s_k) = d_{\mathrm{E}}(s_j, s_k)/E_{\max} \tag{8}$$

where N and $E_{\max}$ denote the number of torsions and the maximum of potential energy in the distinguishable structures, respectively. It is seen that the normalization ensures that $\bar{d}_{\mathrm{D}} \in [0,1]$ and $\bar{d}_{\mathrm{E}} \in [0,1]$.

2.3. Nearest Neighborhood Method. In the present method, there is no strict requirement for the selection of N (the number of coupled torsions) in generating the initial-guess structures of local minima. In principle, a better result would be obtained for a larger N (up to the total number of torsions), however, the total number of initial-guess structures will increase according to 3^N. The MS-2DT method[39] assumes that any two torsions are coupled and reduce the total number of initial-guess structures to $9N(N-1)/2$, which quadratically increases with N. Considering that nearby torsions often have relatively stronger coupling than those being far away,[49] but may not be good for ring-structured molecules, we proposed to use the so-called nearest neighborhood method to generate initial-guess structures. Specifically, all N torsions in a molecule are divided into a certain number of groups, each of which contains n neighborhood torsions. For each group, we can generate 3^n initial-guess structures and the total number of initial-guess structures for all groups is about $(N-1)3^n$, which is significantly smaller than 3^N for $n < N$. In the following text, we denote the method with n nearest neighborhood torsions by nNN. It is noted that the MS-2DT method is not a special case of the nearest neighborhood method because every two (not every two neighbors) torsions are assumed to be coupled.

For the purpose of validating the proposed MS-T(nNN) method, the present study adopted the simplest non-trivial scenario of $n = 2$, since $n = 1$ would result in the trivial case where all torsions are uncoupled, as shown in Figure 1. Take n-decane again as an example (excluding methyl group), the number of initial-guess structures by MS-T, MS-2DT, and the present MS-T(2NN) method are $3^7 = 2189$, $C_7^2 \times 3^2 = 189$, and $(7-1) \times 3^2 = 54$, respectively. It is apparent that the MS-T(2NN) method reduces greatly the computational cost compared to the other two methods. The comparison of their computational results for partition functions will be presented and their performance will be assessed by using the proposed metric-based method in the following section. It should be noted that the present metric-based method can be combined with any method for generating initial-guess structures.

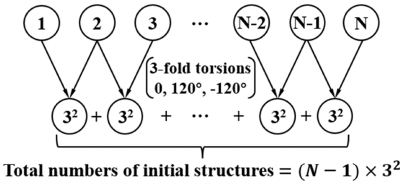

Figure 1. Schematic of the simplest variant MS-T(2NN) (two nearest neighborhood torsions are coupled) method to generate initial-guess structures.

2.4. Electronic Structure Method. To validate the present computational methods, we considered the large straight-chain alkane molecules n-C_nH_{2n+2} (n = 6−10). The geometries optimization and vibrational frequencies of the stationary points for the hydrogen abstraction reactions of n-C_nH_{2n+2} + H (n = 6−7) and larger n-alkanes molecules (from C_8 to C_{10}) were calculated at B3LYP/6-311++G(d,p) level.[50] All the calculations were performed with the Gaussian 09 program package[51] and the optimized geometries of all distinguishable structures were provided in the Supporting Information.

3. RESULTS AND DISCUSSION

3.1. Structures Generation by MS-T(2NN) and MS-T. For the comparison between the MS-T and MS-T(2NN) methods, we studied the hydrogen abstraction reactions of n-hexane and n-heptane by H atom. The MS-T method is too computationally expensive for larger systems such as n-octane, n-nonane, and n-decane, which were studied by the MS-T(2NN) method only. Table 1 summarizes the number of distinguishable structures for all reactants and transition states of the hydrogen abstraction reactions of n-C_nH_{2n+2} + H (n = 6−7) using the MS-T and MS-T(2NN) methods.

Table 1. Number of Distinguishable Structures for Reactants and Transition States (Excluding Mirror-Image Structures)

	MS-T	MS-T(2NN)
n-hexane	9	5
n-hexane-TS1	28	14
n-hexane-TS2	17	11
n-hexane-TS3	17	11
n-heptane	22	7
n-heptane-TS1	65	17
n-heptane-TS2	41	15
n-heptane-TS3	41	15
n-heptane-TS4	22	8

As an example of reactants, the n-heptane molecule has six torsions that are associated with internal rotations around the six C−C single bonds. The seven carbon atoms of n-heptane are labeled as $H_3C^{(1)}-H_2C^{(2)}-H_2C^{(3)}-H_2C^{(4)}-H_2C^{(5)}-H_2C^{(6)}-H_3C^{(7)}$. Excluding the first and the last methyl groups, the rest of the four torsions are considered for generating initial-guess structures. Therefore, 81 initial-guess structures were generated by the MS-T method and 27 initial-guess

https://doi.org/10.1021/acs.jpca.2c04724
J. Phys. Chem. A 2022, 126, 8305−8314

structures were generated by the MS-T(2NN) method. The total number of distinguishable structures (excluding mirror-image structures) are 22 by the MS-T method and 7 by the MS-T(2NN) method.

As an example of transition states, the *n*-heptane-TS1, an H atom in the methyl group was abstracted by H radical. The seven carbon atoms of *n*-heptane-TS1 are labeled as $H_3C^{(1)}$–$H_2C^{(2)}$–$H_2C^{(3)}$–$H_2C^{(4)}$–$H_2C^{(5)}$–$H_2C^{(6)}$–$H_3C^{(7)}$–H. Excluding the $H_3C^{(1)}$ methyl group, 243 initial-guess structures were generated by the MS-T method and 36 initial-guess structures were generated by the MS-T(2NN) method. The total number of distinguishable structures (excluding mirror-image structures) are 65 by the MS-T method and 17 by the MS-T(2NN) method.

Tables 2 and 3 list all distinguishable structures of *n*-heptane and *n*-heptane-TS1 identified by using the MS-T and MS-T(2NN) methods in the ascending sort order of the energy metric with respect to the benchmark structure (the lowest-energy structures, labeled as S1). The complete structural information for the other molecules and transition states are given in the Supporting Information. It is seen that the distinguishable structures generated by the MS-T(2NN) method form a small subset of those generated by the MS-T method.

Table 2. Structural Information (in the Ascending Order of Energy Metric) for *n*-Heptane Using the MS-T and MS-T(2NN) (in Bold Red) Methods (Units in kcal/mol for Energy and Degree for Dihedral Angles)

	torsion				$d_D(s_1,s_j)$	energy	$d_E(s_1,s_j)$
structure	$C^{(2)}$–$C^{(3)}$	$C^{(3)}$–$C^{(4)}$	$C^{(4)}$–$C^{(5)}$	$C^{(5)}$–$C^{(6)}$	$(\bar{d}_D(s_1,s_j))$		$(\bar{d}_E(s_1,s_j))$
S1	180.00	180.00	180.00	180.00	0.00(0.00)	0.00	0.00(0.00)
S2	179.85	-179.90	177.20	66.11	116.95(0.16)	0.85	0.85(0.13)
S3	179.83	176.71	66.32	176.62	120.53(0.17)	0.89	0.89(0.14)
S4	179.86	175.94	63.75	62.64	237.81(0.33)	1.63	1.63(0.26)
S5	176.95	63.89	63.89	176.95	238.31(0.33)	1.69	1.69(0.27)
S6	65.08	176.31	176.31	65.08	237.22(0.33)	1.71	1.71(0.27)
S7	66.63	177.25	-177.25	-66.63	232.24(0.32)	1.72	1.72(0.27)
S8	177.12	67.17	173.62	66.86	235.23(0.33)	1.73	1.73(0.27)
S9	176.76	67.14	179.40	-66.79	229.91(0.32)	1.81	1.81(0.29)
S10	175.96	62.77	60.58	62.39	358.30(0.50)	2.47	2.47(0.39)
S11	66.18	173.15	64.00	63.20	353.46(0.49)	2.50	2.50(0.39)
S12	67.72	-177.38	-62.74	-62.35	349.81(0.49)	2.59	2.59(0.41)
S13	175.55	64.65	-93.30	-179.60	206.90(0.29)	3.29	3.29(0.52)
S14	62.65	59.07	59.07	62.65	476.57(0.66)	3.31	3.31(0.52)
S15	179.40	174.29	64.51	-91.04	210.76(0.29)	3.36	3.36(0.53)
S16	178.31	91.13	-66.09	-63.61	320.86(0.45)	4.15	4.15(0.65)
S17	66.19	171.96	66.29	-90.24	325.31(0.45)	4.23	4.23(0.67)
S18	176.01	63.24	65.12	-90.13	325.50(0.45)	4.25	4.25(0.67)
S19	68.05	-176.85	-63.56	93.32	318.22(0.44)	4.31	4.31(0.68)
S20	64.62	65.11	-93.72	-69.64	426.90(0.59)	5.06	5.06(0.80)
S21	62.59	61.14	66.88	-89.36	440.02(0.61)	5.07	5.07(0.80)
S22	63.79	-93.58	-93.58	63.79	405.25(0.56)	6.34	6.34(1.00)

Table 3. Structural Information (in the Ascending Order of Energy Metric) for *n*-Heptane-TS1 Using the MS-T and MS-T(2NN) (in Bold Red) Methods (Units in kcal/mol for Energy and Degree for Dihedral Angles)

	Torsion					$d_D(s_1,s_j)$	Energy	$d_E(s_1,s_j)$
Structure	$C^{(2)}$-$C^{(3)}$	$C^{(3)}$-$C^{(4)}$	$C^{(4)}$-$C^{(5)}$	$C^{(5)}$-$C^{(6)}$	$C^{(6)}$-$C^{(7)}$	$(\bar{d}_D(s_1,s_j))$		$(\bar{d}_E(s_1,s_j))$
S1	-179.89	-179.68	-179.59	-179.97	66.18	0.00(0.00)	0.00	0.00(0.00)
S2	180.00	-180.00	-180.00	-180.00	179.99	114.67(0.13)	0.05	0.05(0.01)
S3	179.86	-180.00	176.95	65.62	175.35	227.60(0.25)	0.79	0.79(0.15)
S4	66.09	177.77	-179.84	179.68	65.65	117.70(0.13)	0.84	0.84(0.15)
S5	176.67	66.90	176.70	179.42	65.23	122.12(0.14)	0.85	0.85(0.16)
S6	66.27	177.91	-179.86	-178.36	-65.49	122.51(0.14)	0.86	0.86(0.16)
S7	179.99	176.75	66.78	175.80	65.21	249.78(0.28)	0.86	0.86(0.16)
S8	176.71	66.69	176.23	-179.37	-65.70	119.12(0.13)	0.87	0.87(0.16)
S9	179.77	-179.90	177.45	66.73	63.88	252.20(0.28)	0.87	0.87(0.16)
S10	179.91	176.77	66.47	177.41	-65.71	253.68(0.28)	0.87	0.87(0.16)
S11	66.34	177.12	-179.96	179.60	179.93	231.52(0.26)	0.89	0.89(0.16)
S12	-179.96	176.84	66.91	176.87	-179.35	234.67(0.26)	0.92	0.92(0.17)
S13	176.61	66.43	176.82	179.76	-179.80	235.27(0.26)	0.93	0.93(0.17)
S14	179.94	-179.91	177.24	66.96	-75.65	258.46(0.29)	1.12	1.12(0.21)
S15	-179.99	176.12	63.57	62.03	175.59	348.54(0.39)	1.56	1.56(0.29)
S16	179.99	176.14	64.11	63.40	63.51	239.89(0.27)	1.61	1.61(0.30)
S17	63.37	63.85	175.35	-179.59	-65.86	370.70(0.41)	1.62	1.62(0.30)
S18	62.27	62.71	176.71	179.27	65.77	240.31(0.27)	1.64	1.64(0.30)
S19	65.73	177.05	176.80	65.41	175.47	345.16(0.38)	1.65	1.65(0.30)
S20	66.50	177.27	-177.34	-66.21	-175.38	351.11(0.39)	1.65	1.65(0.30)
S21	176.88	67.06	173.80	66.19	176.02	346.77(0.39)	1.66	1.66(0.31)
S22	176.03	63.11	63.20	175.50	65.68	243.52(0.27)	1.66	1.66(0.31)
S23	176.83	63.62	64.15	178.08	-65.32	369.68(0.41)	1.67	1.67(0.31)
S24	62.70	64.19	176.59	179.99	-179.95	351.28(0.39)	1.68	1.68(0.31)
S25	175.62	62.79	63.46	176.19	-179.83	356.79(0.40)	1.69	1.69(0.31)
S26	66.24	177.36	177.24	66.59	63.94	235.67(0.26)	1.70	1.70(0.31)
S27	65.71	176.68	-178.06	-67.41	-64.41	362.72(0.40)	1.71	1.71(0.31)
S28	66.51	173.50	67.02	176.41	65.74	237.87(0.26)	1.72	1.72(0.32)
S29	66.63	173.51	66.98	177.84	-65.86	367.95(0.41)	1.73	1.73(0.32)
S30	176.77	66.85	174.59	67.05	64.08	237.70(0.26)	1.74	1.74(0.32)
S31	176.86	67.49	-179.64	-65.75	-174.98	349.17(0.39)	1.74	1.74(0.32)
S32	65.77	173.62	66.78	176.65	-179.35	352.52(0.39)	1.77	1.77(0.33)
S33	66.66	-179.29	-67.15	-177.43	65.55	229.47(0.25)	1.78	1.78(0.33)
S34	66.91	-178.83	-67.04	-176.13	-65.36	361.98(0.40)	1.78	1.78(0.33)
S35	176.46	66.38	178.47	-68.47	-64.52	361.72(0.40)	1.79	1.79(0.33)
S36	179.92	176.28	64.01	65.35	-74.27	375.76(0.42)	1.81	1.81(0.33)
S37	66.78	-179.16	-67.34	-177.16	179.33	342.05(0.38)	1.87	1.87(0.34)
S38	66.57	177.48	177.37	66.82	-75.69	374.49(0.42)	1.95	1.95(0.36)
S39	66.42	177.10	-177.33	-67.62	75.42	240.75(0.27)	1.97	1.97(0.36)
S40	176.55	66.79	173.57	67.54	-74.95	377.53(0.42)	1.99	1.99(0.37)
S41	176.85	67.31	-179.83	-66.41	76.35	240.22(0.27)	2.05	2.05(0.38)
S42	175.97	62.83	59.90	62.04	175.21	469.14(0.52)	2.43	2.43(0.45)
S43	62.84	63.56	173.10	65.39	175.81	465.60(0.52)	2.43	2.43(0.45)
S44	176.13	62.67	60.87	63.23	62.87	361.28(0.40)	2.44	2.44(0.45)
S45	62.59	60.89	63.81	176.58	66.21	357.01(0.40)	2.44	2.44(0.45)
S46	66.14	172.96	63.62	62.53	175.02	464.45(0.52)	2.45	2.45(0.45)
S47	62.23	60.35	63.01	177.66	-65.62	489.42(0.54)	2.45	2.45(0.45)
S48	66.04	173.17	63.73	63.62	63.63	356.85(0.40)	2.49	2.49(0.46)
S49	62.83	63.66	178.23	-66.48	-175.54	467.86(0.52)	2.50	2.50(0.46)
S50	62.25	60.09	63.39	176.19	-179.68	466.90(0.52)	2.52	2.52(0.46)
S51	66.97	-178.24	-63.51	-62.73	-174.82	356.10(0.40)	2.52	2.52(0.46)
S52	63.25	64.07	173.21	66.74	63.68	473.07(0.53)	2.52	2.52(0.46)
S53	62.96	64.20	179.20	-67.25	-64.45	477.82(0.53)	2.56	2.56(0.47)
S54	67.90	-176.49	-62.26	-62.70	-63.06	479.24(0.53)	2.58	2.58(0.48)
S55	175.93	63.77	62.58	64.68	-75.29	495.36(0.55)	2.71	2.71(0.50)
S56	66.60	-179.18	-65.09	-64.14	75.72	353.89(0.39)	2.75	2.75(0.51)
S57	62.89	64.11	173.45	67.73	-75.32	494.19(0.55)	2.77	2.77(0.51)
S58	65.31	170.73	64.94	66.35	-75.15	494.86(0.55)	2.81	2.81(0.52)
S59	62.16	64.31	-179.61	-65.81	77.24	359.20(0.40)	2.81	2.81(0.52)
S60	62.21	60.41	60.43	62.48	174.54	583.69(0.65)	3.19	3.19(0.59)
S61	62.87	60.06	60.53	62.99	63.11	477.48(0.53)	3.26	3.26(0.60)
S62	62.47	60.97	62.77	65.83	-74.65	609.65(0.68)	3.45	3.45(0.64)
S63	179.72	-72.66	-100.45	62.41	62.40	307.97(0.34)	4.28	4.28(0.79)
S64	179.35	71.50	94.81	-64.97	75.49	319.48(0.35)	4.56	4.56(0.84)
S65	66.07	68.70	92.89	-66.35	77.52	438.13(0.49)	5.43	5.43(1.00)

3.2. Verification of the Qualitative MS-T(2NN) Method Based on the Voronoi Tessellation. In our previous study[49] about the MS-T method, we proposed an improved method (MS-ASB) to approximately reconstruct the torsional potential energy surface based on the Voronoi tessellation. One of the important findings in the study is that the extent of torsional anharmonicity is correlated with the non-uniform distribution of local minima in the coordinate space of dihedrals. In the present study, we applied this understanding to examine the nearest neighborhood approximation.

https://doi.org/10.1021/acs.jpca.2c04724
J. Phys. Chem. A 2022, 126, 8305−8314

For *n*-heptane, four torsions, $C^{(2)}-C^{(3)}$, $C^{(3)}-C^{(4)}$, $C^{(4)}-C^{(5)}$, and $C^{(5)}-C^{(6)}$, are considered in the MS-T method. The present 2NN approximation considered only two distinct combinations, [$C^{(2)}-C^{(3)}$, $C^{(3)}-C^{(4)}$] and [$C^{(3)}-C^{(4)}$, $C^{(4)}-C^{(5)}$], as adjacent coupled torsions. As shown in Figure 2i, it

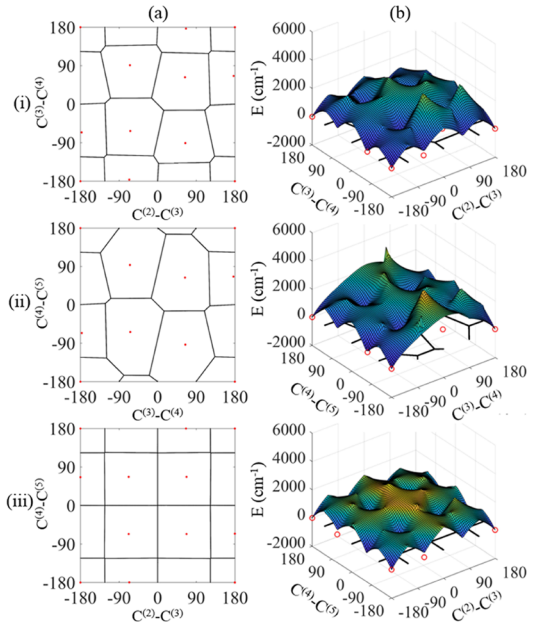

Figure 2. (a) Weighted the Voronoi tessellation and (b) reconstructed potential energy surface based on the method.[49]

can be clearly seen that the coupling of [$C^{(2)}-C^{(3)}$, $C^{(3)}-C^{(4)}$] results in a non-uniform distribution of local minima so that there is no strict periodic variation along either the $C^{(2)}-C^{(3)}$ coordinate or the $C^{(3)}-C^{(4)}$ coordinate. Similar non-uniformity of local minima can be also seen in Figure 2ii due to the coupling of [$C^{(3)}-C^{(4)}$, $C^{(4)}-C^{(5)}$]. The torsions $C^{(2)}-C^{(3)}$ and $C^{(4)}-C^{(5)}$ are assumed to be uncoupled according to the present 2NN approximation. As a comparison, the Voronoi tessellation for the local minima generated by the [$C^{(2)}-C^{(3)}$, $C^{(4)}-C^{(5)}$] is shown in Figure 2iii. Apparently, the distribution of local minima is quite uniform and the periodic variation along each coordinate is well retained, implying the decoupling of these two torsions. It should be noted that the above examined case of *n*-heptane does not contain SC torsions. For the systems containing SC torsions, such as the molecules with the various functional groups or the transition state structures, the larger nearest neighborhood approximations (e.g., 3NN or 4NN) may be needed for satisfactory results. Besides, it also should be noted that, in the MS-T method, the Voronoi tessellation for the complete set of structures guarantees the method will have the correct low-temperature limit (quantum HO) and high-temperature limit (classical torsional integral). If the method with a subset of structures, such as the MS-T(2NN) method, it may not retain these limits. Whether the method with a small subset of structures guarantees the limits is to be studied in our future work.

3.3. Partition Function and Standard State Entropy. The comparison of the partition function ratio of all reactants and transition states of the hydrogen abstraction reactions, *n*-C_nH_{2n+2} + H (n = 6–7), using the MS-T and MS-T(2NN) methods are shown in Figure 3. As expected, the MS-T(2NN) method predicts smaller values of the partition function for it

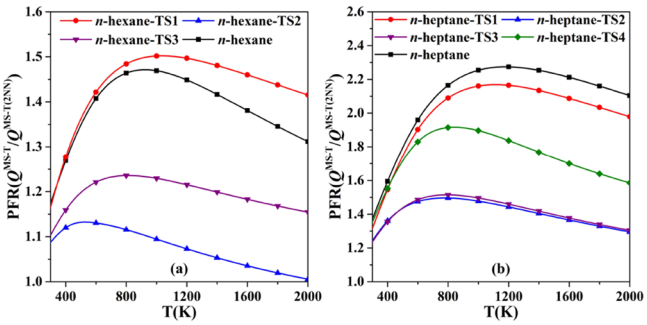

Figure 3. Partition function ratio (PFR), $Q^{MS-T}/Q^{MS-T(2NN)}$, using the MS-T and MS-T(2NN) methods for (a) *n*-hexane and *n*-hexane-TS1 to TS3 and (b) *n*-heptane and *n*-heptane-TS1 to TS4.

considers only a subset of the structures considered by the MS-T method. Surprisedly, the differences between the predictions of these two methods are not significant. Specifically, the partition function ratio, PFR = $Q^{MS-T}/Q^{MS-T(2NN)}$, is generally less than 1.5 for *n*-hexane and its transition states and 2.2 for *n*-heptane and its transition states in the range of 300–2000 K, whereas the number of distinguishable structures by the MS-T(2NN) is significantly smaller than the MS-T method. Therefore, it can be deduced that the MS-T(2NN) method is able to generate the important structures, which make a dominant contribution to the partition function calculation.

To further validate the MS-T(2NN) method, we also calculated the standard state entropy, which is derived from the partition function as follows:

$$S = k_B \ln Q - \frac{1}{T}\left(\frac{\partial \ln Q}{\partial \beta}\right) \tag{9}$$

The calculated entropies using the MS-T and MS-T(2NN) methods for *n*-alkanes (from C_6 to C_{10}) and the available reference data[52] in the range of 298–2000 K are summarized in Table 4.

Generally, the calculated entropies using either the MS-T method or the MS-T(2NN) method are slightly less than the reference data. For *n*-hexane and *n*-heptane, the entropies calculated by the MS-T method agree very well with the reference data and the differences are less than 1%. Although the MS-T(2NN) method has very few structures than the MS-T method, its entropy predictions also agree well with the reference data with the relative errors being less than 2%. We used the MS-T(2NN) method to study the larger *n*-alkanes (from C_8 to C_{10}), for which the MS-T method is computationally unaffordable. It is seen that the differences between the MS-T(2NN) predictions and the reference data slightly increase with the molecule size, but the relative errors are less than 5% from 298 to 1500 K. It is again demonstrated that the present method is capable of generating results with acceptable accuracy for a much lower computational cost compared with the MS-T method.

3.4. Distribution of Energy and Dihedral Metrics. The preceding sections have shown that the present method can predict partition functions with acceptable accuracy by using a small subset of structures generated by the MS-T method. To understand this result, we can make use of the concepts of energy and dihedral metrics that we introduced in Section 2.2.

For *n*-heptane, 22 and 7 distinguishable structures are identified by the MS-T and MS-T(2NN) methods, respec-

https://doi.org/10.1021/acs.jpca.2c04724
J. Phys. Chem. A 2022, 126, 8305–8314

Table 4. Standard State Entropy (in cal/mol/K) of *n*-Alkanes (from C_6 to C_{10}) at 298.15−2000 K Calculated Using the MS-T and MS-T(2NN) Methods and Compared with the Reference Data[52a]

		standard entropy at different temperatures				
molecule	method	298.15 K	500 K	1000 K	1500 K	2000 K
n-hexane	MS-T	92.21 (0.8%)	114.37 (0.4%)	159.70 (0.5%)	194.49 (0.5%)	222.05
	MS-T(2NN)	91.36 (1.7%)	113.26 (1.4%)	159.01 (0.9%)	194.21 (0.6%)	222.00
	Ref. data	92.91	114.84	160.5	195.4	
n-heptane	MS-T	101.47 (0.8%)	127.27 (0.4%)	179.93 (0.3%)	220.24 (0.1%)	252.12
	MS-T(2NN)	99.81 (2.4%)	125.10 (2.1%)	178.10 (1.3%)	218.93 (0.7%)	251.18
	Ref. data	102.29	127.72	180.5	220.5	
n-octane	MS-T(2NN)	107.87 (3.4%)	136.38 (3.0%)	196.83 (1.8%)	243.55 (0.9%)	280.38
	Ref. data	111.67	140.61	200.4	245.7	
n-nonane	MS-T(2NN)	115.63 (4.5%)	147.41 (4.0%)	215.22 (2.4%)	267.72 (1.1%)	309.10
	Ref. data	121.04	153.49	220.4	270.8	
n-decane	MS-T(2NN)	123.56 (5.3%)	158.55 (4.7%)	233.61 (2.9%)	291.88 (1.4%)	337.84
	Ref. data	130.42	166.38	240.5	296.0	

[a]In the brackets are the relative errors with respect to the reference data.

tively. Therefore, we can form C_{22}^2= 231 and C_7^2= 21 pairs of structures for the two methods. Each pair of the *j*th and *k*th structures has s dihedral metric $\overline{d}_D(s_j, s_k)$ and an energy metric $\overline{d}_E(s_j, s_k)$. We can show all identified structures in the Cartesian space of the metrics as shown in Figure 4a, where each point presents a pair of structures (denoted by the subscript "*j*" and "*k*") and has the coordinates $(\overline{d}_E(s_j, s_k), \overline{d}_D(s_j, s_k))$.

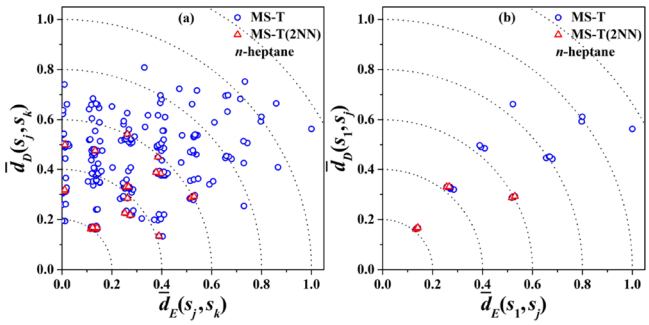

Figure 4. Distributions of distinguishable structures of *n*-heptane in the space of $\overline{d}_D$ and $\overline{d}_E$ using the MS-T and MS-T(2NN) methods for different coordinates (a) $(\overline{d}_E(s_j, s_k), \overline{d}_D(s_j, s_k))$ and (b) $(\overline{d}_E(s_1, s_j), \overline{d}_D(s_1, s_j))$.

Although Figure 4a can represent the "similarity" or "closeness" of any two structures, it does not provide information about the relative importance of each structure to the prediction of partition functions. As discussed in the Introduction Section, those structures that are sufficiently "close" to the lowest energy conformer are more important than those being "far" from it. Consequently, we replotted the figure by presenting each distinguishable structure in terms of its metrics with respect to the lowest energy conformer (denoted by the subscript "1"), as shown in Figure 4b, where each point presents a structure (denoted by the subscript "*j*") has the coordinates $(\overline{d}_E(s_1, s_j), \overline{d}_D(s_1, s_j))$. In the new representation, those being closer to the origin (representing the lowest energy conformer) make larger contributions to the partition function calculation than those being farther from the origin. It is clearly seen that the structures generated by the MS-T(2NN) method are all close to the origin but quite a number of structures generated by the MS-T method are far from the origin. Consequently, the good performance of the MS-T(2NN) method can be understood by that it contains a small but important subset of the structures and that a full set of distinguishable structures may be unnecessary for calculations with a certain tolerance of errors. The same observation and interpretation apply to the four transition states of *n*-heptane, as shown in Figure 5, and to *n*-hexane and its transition states, as shown in Figure 6.

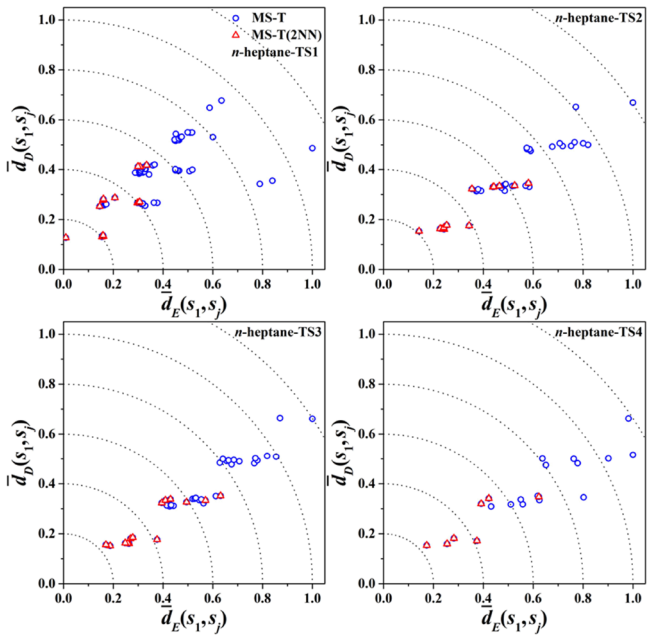

Figure 5. Distribution of distinguishable structures (with respect to the lowest energy conformer) in the space of $\overline{d}_D$ and $\overline{d}_E$ using the MS-T and MS-T(2NN) methods for *n*-heptane-TS1 to TS4.

3.5. Comparison of MS-2DT and MS-3DT with MS-T.

We can use the above developed metric-based method to assess the performance of other methods, for example, the MS-2DT (any two torsions are assumed to be coupled) method of Wu et al.[39] and the MS-3DT (any three torsions are assumed to be coupled) method following the same idea. Compared with the present MS-T(2NN) method, these two methods generate larger subsets of the structure set generated by the

https://doi.org/10.1021/acs.jpca.2c04724
J. Phys. Chem. A 2022, 126, 8305−8314

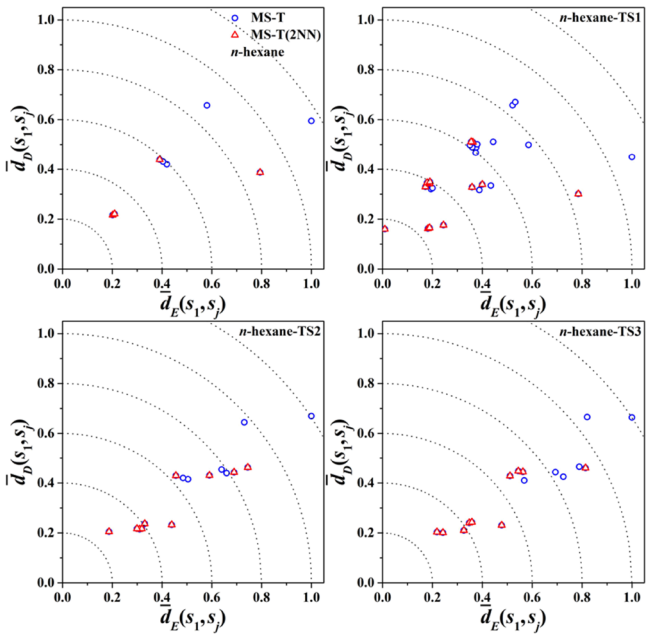

Figure 6. Distribution of distinguishable structures (with respect to the lowest energy conformer) in the space of $\bar{d}_D$ and $\bar{d}_E$ using the MS-T and MS-T(2NN) methods for *n*-hexane and *n*-hexane-TS1 to TS3.

MS-T method. The inclusion relation of these subsets is MS-T(2NN) ⊆ MS-2DT ⊆ MS-3DT ⊆ MS-T.

For *n*-heptane, there are 11 and 18 distinguishable structures (excluding mirror-image structures) generated by MS-2DT and MS-3DT, respectively. For *n*-heptane-TS1, there are 32 and 55 distinguishable structures (excluding mirror-image structures) generated by MS-2DT and MS-3DT, respectively. As expected, more structures can make the calculations more accurate. Figure 7 shows that the partition function ratio of

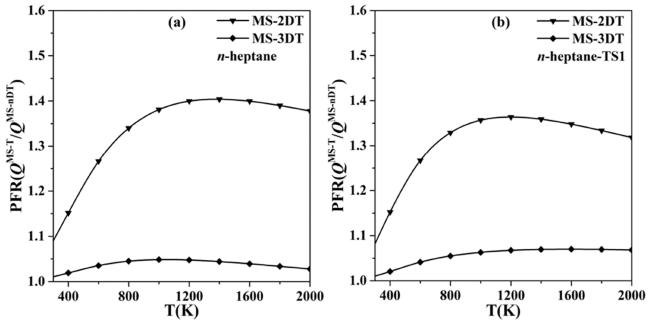

Figure 7. Partition function ratio (PFR) of Q^{MS-T}/Q^{MS-nDT} using the MS-T and MS-*n*DT methods for (a) *n*-heptane and (b) *n*-heptane-TS1.

Q^{MS-T}/Q^{MS-2DT} is less than 1.4 for both cases of *n*-heptane and *n*-heptane-TS1, and the similar small ratios were obtained for other systems. Furthermore, the partition function ratio of Q^{MS-T}/Q^{MS-3DT} is as small as 1.1 for all the cases considered in the present study.

To understand the good performance of MS-2DT and MS-3DT, we compared their metric distributions with that of MS-T in Figure 8. Again, it is seen that the structures generated by MS-2DT and MS-3DT are concentrated in the region close to the origin and that the structures of MS-3DT occupy a larger region and therefore generate better predictions than MS-2DT.

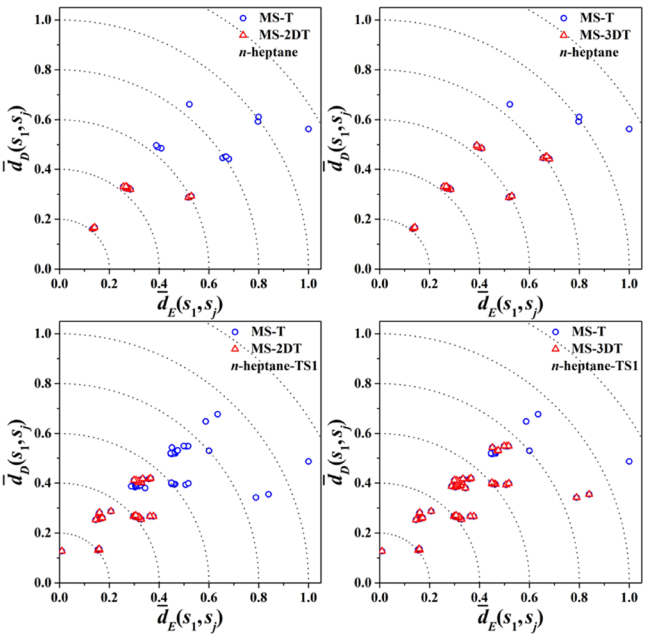

Figure 8. Distribution of distinguishable structures (with respect to the lowest energy conformer) in the space of $\bar{d}_D$ and $\bar{d}_E$ using the MS-T and MS-*n*DT methods for *n*-heptane and *n*-heptane-TS1.

Consequently, the present metric-based method can be considered as a useful measure to assess the "quality" of a subset for the partition function calculation.

4. CONCLUSIONS

The MS-T method proposed by Zheng et al.,[30] and the related open-source code MSTor,[32,33] has been proved to be an effective tool for calculating partition functions of large molecules, where the torsional modes are often coupled so that the widely-used one-dimensional hindered rotor (1D-HR) treatment is inapplicable. The MS-T method has a few great advantages, such as avoiding evaluating high-dimensional integrals and establishing a one-to-one correspondence between the low-frequency torsions and normal modes. However, it requires identifying all local minima (and even saddle points) on the torsional potential energy surface, which often results in a huge number of geometry optimization calculations for large molecules. Several variants of MS-T have been proposed to reduce the number of geometry optimization calculations by considering subsets of the complete set of all local minima. The remaining issue to be addressed is that what kinds of subsets can predict the partition function with acceptable accuracy and less computational cost.

In the present work, we proposed a metric-based method to assess the performance of various variants of the MS-T method for calculating the conformational−rovibrational partition function. The central idea of the method is to mathematically quantify the concept of "similarity" of two torsional conformers by defining the dihedral and energy metrics between the two conformers. Consequently, two torsional conformers are "similar" if they have close dihedral and energy metrics. Furthermore, a torsional conformer is considered important in the partition function calculation if it is "similar" to the lowest-energy conformer. The underlying physics is based on that those torsional conformers with lower energies have larger contributions to the partition function according to the Boltzmann factor in the definition of the partition function.

https://doi.org/10.1021/acs.jpca.2c04724
J. Phys. Chem. A 2022, 126, 8305−8314

We first compared the MS-T method with the proposed MS-T(2NN) method, which can be treated as the simplest variant of the former by considering the coupling of MS-T(2NN). The results show that the MS-T(2NN) method agrees with the MS-T method in the systems of n-C_nH_{2n+2} + H (n = 6−7) with computational discrepancies being about a factor of two. In addition, the entropy predictions for n-C_nH_{2n+2} (n = 6−10) by MS-T(2NN) agree with the literature data with errors being generally less than 5%. Considering that the MS-T(2NN) method uses a very small subset of the complete set of local minima used in the MS-T method, the above results are astonishing. Our metric-based diagnosis indicates that the local minima including in the subset used by the MS-T(2NN) are close to the origin (representing the lowest-energy conformer) in the space of dihedral and energy metrics.

To verify the above findings, we also considered the other two variants of the MS-T method, such as the MS-2DT method, which uses a subset of local minima by considering the coupling of any (unnecessarily nearest) two torsions, and the MS-3DT method, which uses a larger subset of local minima by considering the coupling of any three torsions. As expected, the MS-2DT and MS-3DT methods made increasingly better predictions of the partition functions because they include more local minima "similar" to the lowest-energy conformers.

Overall, the present method provides a mathematically rigorous and computationally effective diagnosis tool to assess various MS-T methods dealing with the torsional anharmonicity of large molecules in the partition function calculation. Further validation for more molecules and reaction systems merits future studies. In addition, the metric-based method may play an important role in identifying the Q(partition function)-important torsional conformers without introducing any coupling assumption and when the complete set of local minima is unavailable.

■ ASSOCIATED CONTENT

Supporting Information

The Supporting Information is available free of charge at https://pubs.acs.org/doi/10.1021/acs.jpca.2c04724.

Optimized Cartesian coordinates and structural information of the distinguishable structures for all species (PDF)

■ AUTHOR INFORMATION

Corresponding Author

Peng Zhang − *Department of Mechanical Engineering, The Hong Kong Polytechnic University, Kowloon 999077, Hong Kong; Department of Mechanical Engineering, City University of Hong Kong, Kowloon 999077, Hong Kong;* orcid.org/0000-0002-1806-4200; Phone: (852) 34429561; Email: penzhang@cityu.edu.hk

Authors

Yicheng Chi − *Department of Mechanical Engineering, The Hong Kong Polytechnic University, Kowloon 999077, Hong Kong;* orcid.org/0000-0002-4301-6059

Qinghui Meng − *Department of Mechanical Engineering, The Hong Kong Polytechnic University, Kowloon 999077, Hong Kong; National Synchrotron Radiation Laboratory, University of Science and Technology of China, Hefei 230052, China*

Chengming He − *Wide Range Flight Engineering Science and Application Center, Institute of Mechanics, Chinese Academy of Sciences, Beijing 100864, China*

Complete contact information is available at: https://pubs.acs.org/10.1021/acs.jpca.2c04724

Notes

The authors declare no competing financial interest.

■ ACKNOWLEDGMENTS

This work was financially supported by the National Natural Science Foundation of China (No. 52176134) and by the Hong Kong Polytechnic University (G-UAHP).

■ REFERENCES

(1) Westbrook, C. K.; Dryer, F. L. Chemical kinetics and modeling of combustion processes. processes. *Proc. Combust. Inst.* **1981**, *18*, 749−767.

(2) Colket, M.; Edwards, T.; Williams, S.; Cernansky, N. P.; Miller, D. L.; Egolfopoulos, F.; Lindstedt, P.; Seshadri, K.; Dryer, F. L.; Law, C. K.; Friend, D.; Lenhert, D. B.; Pitsch, H.; Sarofim, A.; Smooke, M.; Tsang, W.Development of an experimental database and kinetic models for surrogate jet fuels. *45th AIAA Aerospace Sciences Meeting and Exhibit*. 2007 AIAA-2007-0770.

(3) Farrell, J.; Cernansky, N. P.; Dryer, F. L.; Law, C. K.; Friend, D.; Hergart, C.; McDavid, R.; Patel, A.; Mueller, C. J.; Pitsch, H. Development of an experimental database and kinetic models for surrogate diesel fuels. *SAE Tech. Pap.* **2007**, No. 2007-01-0201.

(4) Pitz, W. J.; Cernansky, N. P.; Dryer, F. L.; Egolfopoulos, F.; Farrell, J.; Friend, D. G.; Pitsch, H. Development of an experimental database and chemical kinetic models for surrogate gasoline fuels. *SAE Tech. Pap.* **2007**, No. 2007-01-0175.

(5) Dagaut, P.; Cathonnet, M. The ignition, oxidation, and combustion of kerosene: A review of experimental and kinetic modeling. *Prog. Energy Combust. Sci.* **2006**, *32*, 48−92.

(6) Pitz, W. J.; Mueller, C. J. Recent progress in the development of diesel surrogate fuels. *Prog. Energy Combust. Sci.* **2011**, *37*, 330−350.

(7) Sarathy, S. M.; Farooq, A.; Kalghatgi, G. T. Recent progress in gasoline surrogate fuels. *Prog. Energy Combust. Sci.* **2018**, *65*, 67−108.

(8) Fernández-Ramos, A.; Miller, J. A.; Klippenstein, S. J.; Truhlar, D. G. Modeling the kinetics of bimolecular reactions. *Chem. Rev.* **2006**, *106*, 4518−4584.

(9) Truhlar, D. G.; Garrett, B. C.; Klippenstein, S. J. Current status of transition-state theory. *J. Phys. Chem.* **1996**, *100*, 12771−12800.

(10) Truhlar, D. G.; Hase, W. L.; Hynes, J. T. Current status of transition-state theory. *J. Phys. Chem.* **1983**, *87*, 2664−2682.

(11) Vreven, T.; Byun, K. S.; Komáromi, I.; Dapprich, S.; Montgomery, J. A., Jr.; Morokuma, K.; Frisch, M. J. Combining quantum mechanics methods with molecular mechanics methods in ONIOM. *J. Chem. Theory Comput.* **2006**, *2*, 815−826.

(12) Zhang, L.; Meng, Q.; Chi, Y.; Zhang, P. Toward High-Level Theoretical Studies of Large Biodiesel Molecules: An ONIOM [QCISD (T)/CBS: DFT] Study of the Reactions between Unsaturated Methyl Esters ($C_nH_{2n-1}COOCH_3$) and Hydrogen Radical. *J. Phys. Chem. A* **2018**, *122*, 4882−4893.

(13) Zhang, L.; Zhang, P. Towards high-level theoretical studies of large biodiesel molecules: an ONIOM [QCISD (T)/CBS: DFT] study of hydrogen abstraction reactions of $C_nH_{2n+1}COOC_mH_{2m+1}$ + H. *Phys. Chem. Chem. Phys.* **2015**, *17*, 200−208.

(14) Li, W.; Li, S.; Jiang, Y. Generalized energy-based fragmentation approach for computing the ground-state energies and properties of large molecules. *J. Phys. Chem. A* **2007**, *111*, 2193−2199.

(15) Wu, J.; Ning, H.; Ma, L.; Zhang, P.; Ren, W. Cascaded group-additivity ONIOM: A new method to approach CCSD (T)/CBS

energies of large aliphatic hydrocarbons. *Combust. Flame* **2019**, *201*, 31−43.
(16) Pitzer, K. S.; Gwinn, W. D. Energy levels and thermodynamic functions for molecules with internal rotation I. Rigid frame with attached tops. *J. Chem. Phys.* **1942**, *10*, 428−440.
(17) Pitzer, K. S. Energy levels and thermodynamic functions for molecules with internal rotation: II. Unsymmetrical tops attached to a rigid frame. *J. Chem. Phys.* **1946**, *14*, 239−243.
(18) Kilpatrick, J. E.; Pitzer, K. S. Energy levels and thermodynamic functions for molecules with internal rotation. III. Compound rotation. *J. Chem. Phys.* **1949**, *17*, 1064−1075.
(19) Truhlar, D. G. A simple approximation for the vibrational partition function of a hindered internal rotation. *J. Comput. Chem.* **1991**, *12*, 266−270.
(20) Ayala, P. Y.; Schlegel, H. B. Identification and treatment of internal rotation in normal mode vibrational analysis. *J. Chem. Phys.* **1998**, *108*, 2314−2325.
(21) Ellingson, B. A.; Lynch, V. A.; Mielke, S. L.; Truhlar, D. G. Statistical thermodynamics of bond torsional modes: Tests of separable, almost-separable, and improved Pitzer−Gwinn approximations. *J. Chem. Phys.* **2006**, *125*, No. 084305.
(22) Pfaendtner, J.; Yu, X.; Broadbelt, L. J. The 1-D hindered rotor approximation. *Theor. Chem. Acc.* **2007**, *118*, 881−898.
(23) Lay, T. H.; Krasnoperov, L. N.; Venanzi, C. A.; Bozzelli, J. W.; Shokhirev, N. V. Ab initio study of α-chlorinated ethyl hydroperoxides CH_3CH_2OOH, $CH_3CHClOOH$, and CH_3CCl_2OOH: conformational analysis, internal rotation barriers, vibrational frequencies, and thermodynamic properties. *J. Phys. Chem.* **1996**, *100*, 8240−8249.
(24) Gruzman, D.; Karton, A.; Martin, J. M. L. Performance of Ab Initio and Density Functional Methods for Conformational Equilibria of C_nH_{2n+2} Alkane Isomers (n= 4− 8). *J. Phys. Chem. A* **2009**, *113*, 11974−11983.
(25) Sharma, S.; Raman, S.; Green, W. H. Intramolecular hydrogen migration in alkylperoxy and hydroperoxyalkylperoxy radicals: accurate treatment of hindered rotors. *J. Phys. Chem. A* **2010**, *114*, 5689−5701.
(26) Meng, Q.; Chi, Y.; Zhang, L.; Zhang, P.; Sheng, L. Towards high-level theoretical studies of large biodiesel molecules: an ONIOM/RRKM/Master-equation approach to the isomerization and dissociation kinetics of methyl decanoate radicals. *Phys. Chem. Chem. Phys.* **2019**, *21*, 5232−5242.
(27) Meng, Q.; Zhang, L.; Chen, Q.; Chi, Y.; Zhang, P. Influence of torsional anharmonicity on the reactions of methyl butanoate with hydroperoxyl radical. *J. Phys. Chem. A* **2020**, *124*, 8643−8652.
(28) Van Speybroeck, V.; Van Neck, D.; Waroquier, M. Ab initio study of radical reactions: role of coupled internal rotations on the reaction kinetics (III). *J. Phys. Chem. A* **2002**, *106*, 8945−8950.
(29) Van Speybroeck, V.; Vansteenkiste, P.; Van Neck, D.; Waroquier, M. Why does the uncoupled hindered rotor model work well for the thermodynamics of n-alkanes? *Chem. Phys. Lett.* **2005**, *402*, 479−484.
(30) Zheng, J.; Yu, T.; Papajak, E.; Alecu, I. M.; Mielke, S. L.; Truhlar, D. G. Practical methods for including torsional anharmonicity in thermochemical calculations on complex molecules: The internal-coordinate multi-structural approximation. *Phys. Chem. Chem. Phys.* **2011**, *13*, 10885−10907.
(31) Zheng, J.; Truhlar, D. G. Quantum thermochemistry: Multistructural method with torsional anharmonicity based on a coupled torsional potential. *J. Chem. Theory Comput.* **2013**, *9*, 1356−1367.
(32) Zheng, J.; Meana-Pañeda, R.; Truhlar, D. G. MSTor version 2013: A new version of the computer code for the multi-structural torsional anharmonicity, now with a coupled torsional potential. *Comput. Phys. Commun.* **2013**, *184*, 2032−2033.
(33) Zheng, J.; Mielke, S. L.; Clarkson, K. L.; Truhlar, D. G. MSTor: A program for calculating partition functions, free energies, enthalpies, entropies, and heat capacities of complex molecules including torsional anharmonicity. *Comput. Phys. Commun.* **2012**, *183*, 1803−1812.
(34) Seal, P.; Papajak, E.; Truhlar, D. G. Kinetics of the hydrogen abstraction from carbon-3 of 1-butanol by hydroperoxyl radical: Multi-structural variational transition-state calculations of a reaction with 262 conformations of the transition state. *J. Phys. Chem. Lett.* **2012**, *3*, 264−271.
(35) Seal, P.; Oyedepo, G.; Truhlar, D. G. Kinetics of the Hydrogen atom abstraction reactions from 1-Butanol by hydroxyl radical: theory matches experiment and more. *J. Phys. Chem. A* **2013**, *117*, 275−282.
(36) Zheng, J.; Oyedepo, G. A.; Truhlar, D. G. Kinetics of the hydrogen abstraction reaction from 2-butanol by OH radical. *J. Phys. Chem. A* **2015**, *119*, 12182−12192.
(37) Date, A. W., *Analytic Combustion*; Springer, 2012.
(38) Bao, J. L.; Xing, L.; Truhlar, D. G. Dual-level method for estimating multistructural partition functions with torsional anharmonicity. *J. Chem. Theory Comput.* **2017**, *13*, 2511−2522.
(39) Wu, J.; Ning, H.; Xu, X.; Ren, W. Accurate entropy calculation for large flexible hydrocarbons using a multi-structural 2-dimensional torsion method. *Phys. Chem. Chem. Phys.* **2019**, *21*, 10003−10010.
(40) Halmos, P. R.*A Hilbert space problem book*; Springer Science & Business Media, 2012.
(41) Young, N.*An introduction to Hilbert space*; Cambridge University Press, 2012.
(42) Black, P. E.*Dictionary of Algorithms and Data Structures*; National Institute of Standards and Technology, 1998.
(43) Krause, E. F.*Taxicab geometry: An adventure in non-Euclidean geometry*; Courier Corporation, 1986.
(44) Minkowski, H.*Geometrie der zahlen*; Teubner, 1910.
(45) Rolewicz, S.*Functional analysis and control theory: linear systems*; Springer Science & Business Media, 2013.
(46) Väisälä, J.*Hyperbolic and uniform domains in Banach spaces*; Department of Mathematics, University of Helsinki, 2004.
(47) Xing, L.; Wang, Z.; Truhlar, D. G. Multistructural anharmonicity controls the radical generation process in biofuel combustion. *J. Am. Chem. Soc.* **2019**, *141*, 18531−18543.
(48) Zheng, J.; Meana-Pañeda, R.; Truhlar, D. G. Prediction of experimentally unavailable product branching ratios for biofuel combustion: The role of anharmonicity in the reaction of isobutanol with OH. *J. Am. Chem. Soc.* **2014**, *136*, 5150−5160.
(49) He, C.; Chi, Y.; Zhang, P. Approximate reconstruction of torsional potential energy surface based on voronoi tessellation. *Proc. Combust. Inst.* **2021**, *38*, 757−766.
(50) Beck, A. D. Density-functional thermochemistry. III. The role of exact exchange. *J. Chem. Phys.* **1993**, *98*, 5648−5652.
(51) Frisch, M. J.; Trucks, G. W.; Schlegel, H. B.; Scuseria, G. E; Robb, M. A.; Cheeseman, J. R.; Scalmani, G.; Barone, V.; Mennucci, B.; Petersson, G. A.; Nakatsuji, H.; Caricato, M.; Li, X.; Hratchian, H. P.; Izmaylov, A. F.; Bloino, J.; Zheng, G.; Sonnenberg, J. L.; Hada, M.; Ehara, M.; Toyota, K.; Fukuda, R.; Hasegawa, J.; Ishida, M.; Nakajima, T.; Honda, Y.; Kitao, O.; Nakai, H.; Vreven, T.; Montgomery, J. J. A.; Peralta, J. E.; Ogliaro, F.; Bearpark, M.; Heyd, J. J.; Brothers, E.; Kudin, K. N.; Staroverov, V. N.; Keith, T.; Kobayashi, R.; Normand, J.; Raghavachari, K.; Rendell, A.; Burant, J. C.; Iyengar, S. S.; Tomasi, J.; Cossi, M.; Rega, N.; Millam, J. M.; Klene, M.; Knox, J. E.; Cross, J. B.; Bakken, V.; Adamo, C.; Jaramillo, J.; Gomperts, R.; Stratmann, R. E.; Yazyev, O.; Austin, A. J.; Cammi, R.; Pomelli, C.; Ochterski, J. W.; Martin, R. L.; Morokuma, K.; Zakrzewski, V. G.; Voth, G. A.; Salvador, P.; Dannenberg, J. J.; Dapprich, S.; Daniels, A. D.; Farkas, O.; Foresman, J. B.; Ortiz, J. V.; Cioslowski, J.; Fox, D. J.*Gaussian 09*; Gaussian, Inc.: Wallingford CT, 2009
(52) Scott, D. W.*Chemical Thermodynamic Properties of Hydrocarbons and Related Substances: Properties of the Alkane Hydrocarbons, C1 through C10, in the Ideal Gas State From 0 to 1500 K*; US Department of the Interior, Bureau of Mines, 1974.

https://doi.org/10.1021/acs.jpca.2c04724
J. Phys. Chem. A 2022, 126, 8305−8314